



Early Jurassic long-term oceanic sulfur-cycle perturbations in the Tibetan Himalaya



Zhong Han^{a,b}, Xiumian Hu^{b,*}, Tianchen He^c, Robert J. Newton^c, Hugh C. Jenkyns^d, Robert A. Jamieson^c, Marco Franceschi^e

^a State Key Laboratory of Oil and Gas Reservoir Geology and Exploitation, Institute of Sedimentary Geology, Chengdu University of Technology, Chengdu 610059, China

^b State Key Laboratory of Mineral Deposit Research, School of Earth Sciences and Engineering, Nanjing University, Nanjing 210023, China

^c School of Earth and Environment, University of Leeds, Woodhouse Lane, Leeds LS2 9JT, UK

^d Department of Earth Sciences, University of Oxford, South Parks Road, Oxford OX1 3AN, UK

^e Department of Mathematics and Geosciences, Università degli Studi di Trieste, via Edoardo Weiss, 2, 34128, Trieste, Italy

ARTICLE INFO

Article history:

Received 1 December 2020

Received in revised form 28 September 2021

Accepted 22 October 2021

Available online 20 November 2021

Editor: T. Lyons

Keywords:

sulfur-isotope perturbations
seawater sulfate concentrations
Early Jurassic
carbonate platform
Tibetan Himalaya
southern hemisphere

ABSTRACT

The Early Jurassic is an important interval characterized by several global carbon-isotope ($\delta^{13}\text{C}$) perturbations. Although the $\delta^{13}\text{C}$ records are becoming better documented during this time interval, we have a relatively poor understanding of the associated long-term environmental and climatic changes. In order to decipher these events, we here present new stable sulfur-isotope data of carbonate-associated sulfate ($\delta^{34}\text{S}_{\text{CAS}}$) for the Sinemurian–Pliensbachian interval from the Wölong section in the Tibetan Himalaya that was located palaeogeographically in the southern hemisphere. An overall positive shift in $\delta^{34}\text{S}_{\text{CAS}}$ coincides with the negative $\delta^{13}\text{C}$ excursion around the Sinemurian–Pliensbachian boundary, suggesting an increased ^{34}S -depleted pyrite burial rate. The ensuing overarching negative $\delta^{34}\text{S}_{\text{CAS}}$ shift coincides with the upper Pliensbachian positive $\delta^{13}\text{C}$ excursion. The initial falling limb of the $\delta^{34}\text{S}_{\text{CAS}}$ shift suggests a transient $\delta^{34}\text{S}$ -depleted sulfate input, but this trend was soon reversed to become positive, likely caused by a persistently enhanced ^{32}S -rich pyrite burial flux in the latest Pliensbachian. Modeling results show that maximum oceanic sulfate concentration likely decreased during the Sinemurian–Toarcian interval, probably due to large-scale evaporite deposition in the western Tethys and proto-Atlantic and enhanced pyrite burial in a number of marine settings. The concentration of seawater sulfate could have been high enough to maintain a homogeneous sulfur-isotope ocean in the late Sinemurian, but its persistent decrease may have initiated a spatially heterogeneous ocean after the Pliensbachian: an oceanic geochemical state that was amplified during the Toarcian Oceanic Anoxic Event.

© 2021 Elsevier B.V. All rights reserved.

1. Introduction

The Early Jurassic was a time of large-scale changes in global climate and environment associated with perturbations of the global carbon cycle (e.g. Jenkyns et al., 2002; Jenkyns, 2010; Korte and Hesselbo, 2011; Ruhl et al., 2016; Storm et al., 2020). Examples include the Triassic–Jurassic boundary event (TJBE) and Toarcian Oceanic Anoxic Event (T-OAE) that are coincident with the volcanic activity of the Central Atlantic Magmatic Province (CAMP) and Karoo–Ferrar Large Igneous Provinces, respectively (Blackburn et al., 2013; Burgess et al., 2015). In addition to these two periods of significant carbon-isotope disturbance, also identified by

the volcanogenic fingerprint of mercury in associated organic-rich sediments (Percival et al., 2015, 2017), an increasing number of studies have led to the recognition of other global events within this interval: namely, a Sinemurian–Pliensbachian boundary event (SPBE), a *margaritatus*–*spinatum* zone boundary event (MSBE) accompanied by a negative carbon-isotope excursion (CIE), and a *margaritatus* zone event (ME) characterized by a positive CIE in Europe, northern Africa, eastern Oregon, USA and Tibet, China (e.g. Korte and Hesselbo, 2011; De Lena et al., 2019; Franceschi et al., 2019; Baghli et al., 2020; Storm et al., 2020; Han et al., 2021). Although the carbon-isotope record for this time interval is becoming better documented, uncertainties remain with regard to these carbon-isotope perturbations.

These CIEs have been shown to be associated with major environmental and climatic changes such as warming and cooling, fluctuating redox conditions, ocean acidification, carbonate-platform

* Corresponding author.

E-mail address: huxm@nju.edu.cn (X. Hu).

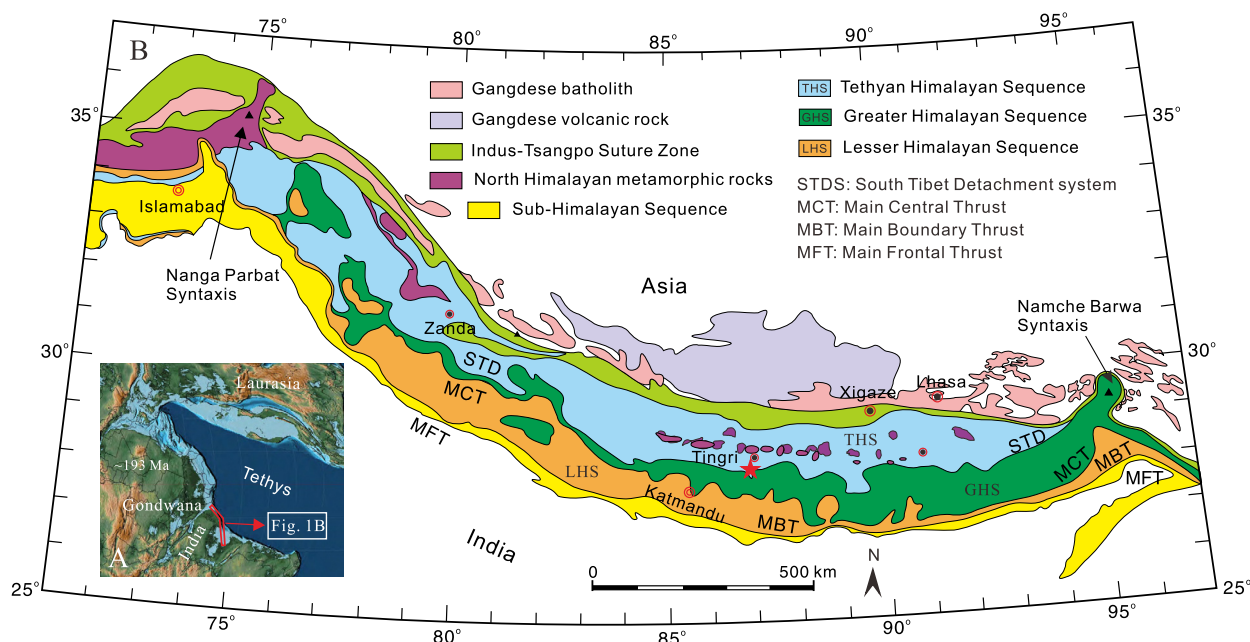


Fig. 1. (A) Early Jurassic palaeogeography showing the northern margin of the Indian subcontinent (red polygon, after Scotese, 2014) and (B) the location of the Wölong section (red star) in the Tethys Himalaya, modified after Guillot et al. (2008). (For interpretation of the colors in the figure(s), the reader is referred to the web version of this article.)

demise and regional sea-level rises and falls that may relate to the impact of varying CO_2 concentrations in the oceans and atmosphere (Hesselbo and Jenkyns, 1998; Franceschi et al., 2014, 2019; Jenkyns, 2020; Müller et al., 2020; Han et al., 2021). The global carbon cycle is intimately tied to the biogeochemical sulfur cycle via organic-matter re-mineralization during microbial sulfate reduction (MSR) and associated pyrite burial (Garrels and Perry, 1974). The study of sulfur-isotope records can thus provide additional information on environmental and climatic changes associated with global CIEs. However, the sulfur cycle has primarily been investigated for certain time windows in the Early Jurassic using isotopes of carbonate-associated sulfate (CAS) as a proxy for sulfate in palaeo-seawater. Studies exist for the lower Toarcian (Gill et al., 2011a; Newton et al., 2011) and, in the case of the Triassic–Jurassic boundary, there are data from both pyrite-sulfur and CAS (Williford et al., 2009; Luo et al., 2018; He et al., 2020). There is therefore a notable gap in records of the long-term evolution of the Early Jurassic sulfur cycle between the TJB and T-OAE, specifically its behavior during the carbon-isotope excursions of the SPBE, ME and MSBE.

Widespread Lower Jurassic carbonate-platform successions from low latitudes of the southeast Neotethys (22 to 26°S) are exposed in the Tibetan Himalaya (Jadoul et al., 1998; Han et al., 2016). In this study, we present new sulfur-isotope data of CAS ($\delta^{34}\text{S}_{\text{CAS}}$) and paired NaOCl leachates ($\delta^{34}\text{S}_{\text{bleach}}$) across the Sinemurian–Pliensbachian interval from the Wölong section in Tibet that, together with existing lower Toarcian $\delta^{34}\text{S}_{\text{CAS}}$ and $\delta^{34}\text{S}_{\text{bleach}}$ data, illustrate the dynamics of the long-term sulfur cycle during a time of Early Jurassic CIE perturbations.

2. Geological setting and stratigraphy

The Tethys Himalaya represents the northern margin of the Indian continent and is now bounded by the Greater Himalaya to the south and by the Yarlung Zangbo Suture Zone to the north (Fig. 1A and B). The Lower Jurassic succession is composed of shallow-water carbonates and siliciclastics in the southern zone, whereas deep-water marls, calcareous shales and silty shales are found in the northern zone (Han et al., 2021 and references therein).

The Wölong section analyzed in this study (Fig. 1B; 28°29'2"N, 87°02'3"E) is located in the southern zone of the Tibetan Tethys Himalaya. The Lower Jurassic has been well constrained in the section by larger benthic foraminifera, the occurrence of *Lithiotis* bivalves, and chemostratigraphy (Jadoul et al., 1998; Han et al., 2016, 2018, 2021). At Wölong, the following lithostratigraphic units are exposed (from the bottom to the top): the Zhamure Formation (upper Sinemurian–lower Pliensbachian), the Pupuga Formation (upper Pliensbachian–lowest Toarcian) and the Nienxiiongla Formation (Toarcian–Aalenian?). Overall, the succession illustrates an evolution that sees a progressive decrease in the terrigenous content of the sediments and an increase of carbonate-rich sediment through time (Jadoul et al., 1998; Han et al., 2016, 2021): (1) The lower Zhamure Formation mainly documents a barrier island-lagoon environment, characterized by mixed carbonate-siliciclastic deposits; (2) the overlying Pupuga Formation gradually passes up-section into shallow-water platform carbonates, dominated by bioclastic grainstones/packstones and yielding *Lithiotis* bivalves; (3) the Nienxiiongla Formation represents a deeper carbonate ramp and is mainly composed of micrites alternating with coarser grained storm-generated layers. The carbon-isotope record from the Wölong section has revealed a series of perturbations that can be correlated with the Sinemurian–Pliensbachian boundary event (SPBE), the *margaritatus* zone event (ME) and *margaritatus*–*spinatum* boundary event (MSBE) (Fig. 2; Han et al., 2021).

3. Material and methods

3.1. CAS and reduced sulfur extraction

Weathered surfaces and visibly altered parts of hand samples were trimmed off prior to powdering, and the residual samples were crushed using a mechanical agate mill. We applied a miniaturized CAS extraction protocol developed recently by He et al. (2019, 2020) to this study. Approximately 6–8 g of powder for each sample were immersed in an excess of 5% NaOCl solution under constant agitation for 72 h to remove the sulfur in organic matter and both sulfate and sulfide minerals. After filtration through

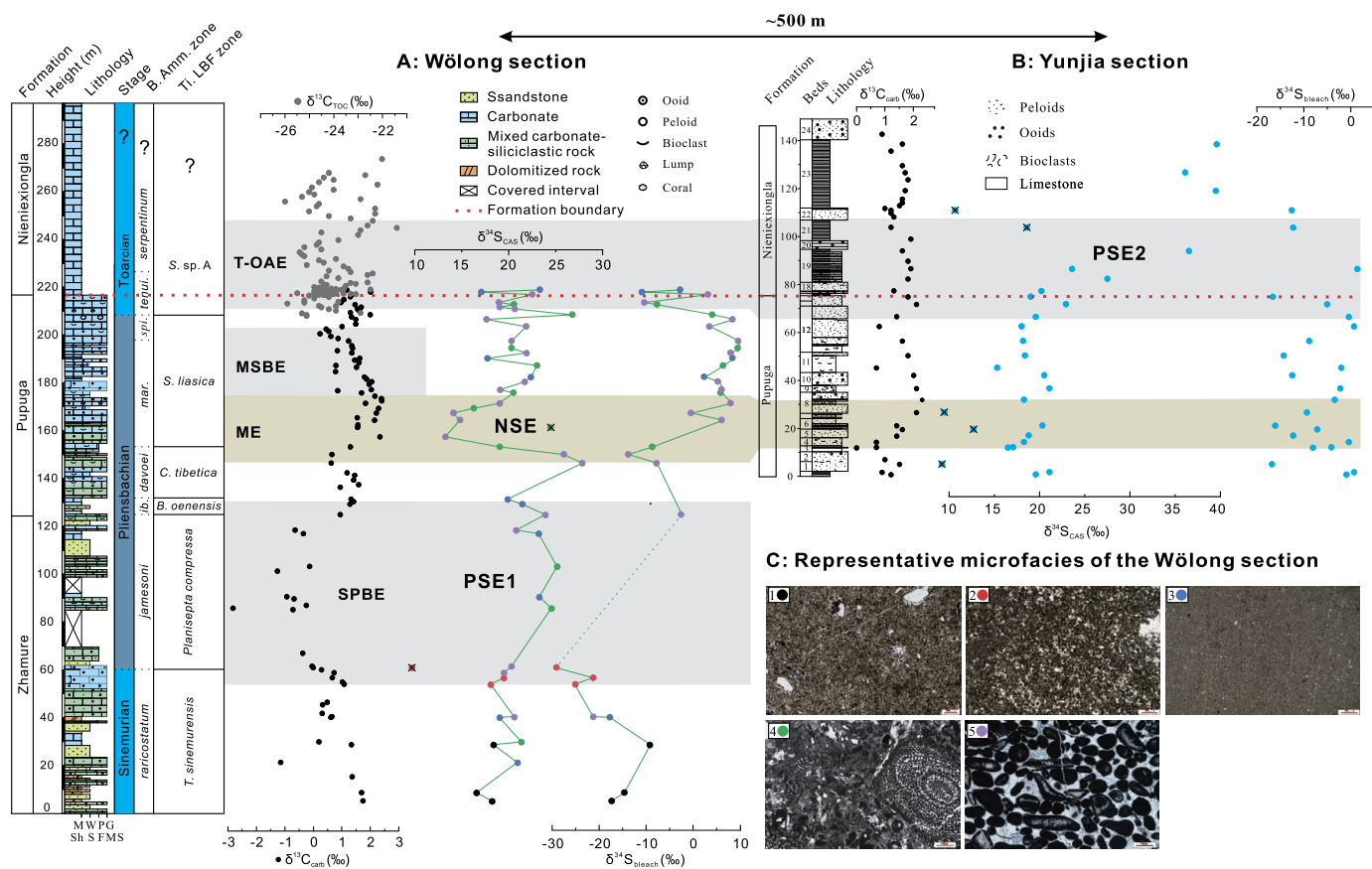


Fig. 2. Lower Jurassic carbon- and sulfur-isotope correlations between the Wölong (A, this study) and Yunjia (B) sections based on the Pupuga–Nienixiongla boundary and trends of carbon and sulfur isotopes. Note that the Yunjia section is located ~500 m away from the Wölong section, see Han et al. (2018, 2021) for details. Wölong section: Sulfur isotopes are from this study and lithological log, biostratigraphical framework, carbon isotopes from Han et al. (2016, 2018, 2021); Yunjia section: Lithological log and carbon and sulfur isotopes are from Wignall et al. (2006) and Newton et al. (2011). Sulfur isotopes of Wölong are illustrated with representative microfacies (C): 1 (black data points): Finely crystalline dolostone; 2 (red data points): Dolomitic packstone/grainstone; 3 (blue data points): Mudstone; 4 (green data points): Wackestone/Packstone; 5 (purple data points): Grainstone. Abbreviations: B. Amm. zone = Boreal ammonite zone; Ti. LBF zone = Tibetan Larger Benthic Foraminiferal zone; Toar. = Toarcian; Tenu. = *Tenuicostatum*; B. oenensis = *Bosniella oenensis*; C. tibetica = *Cyclorbitopsella tibetica*; S. liasica = *Streptocyclamina liasica*; S. sp. A = *Siphovalvulina* sp. A; SPBE = Sinemurian–Pliensbachian boundary event; ME = *margaritatus* zone event; MSBE = *margaritatus*–*spinatum* boundary event; T-OAE = Toarcian Oceanic Anoxic Event; P(N)SIE = Positive (Negative) sulfur-isotope excursion.

a 0.25 μm Polypropylene membrane syringe filter (VWR®), 4 ml of 6 M HCl was added to the NaOCl leachate to produce a solution pH of below 3, after which 2 ml supersaturated BaCl_2 solution was added to trigger BaSO_4 precipitation. The rock residue of each sample was washed 3 times with ultrapure water (18.2 $\text{M}\Omega\cdot\text{cm}$) and subsequently immersed for 24 h in 10% NaCl solution under constant agitation. This H_2O –NaCl rinsing step was repeated five times to completely remove residual sulfate liberated during the NaOCl rinsing step. After these processes, rock residues were rinsed in ultrapure water five times to remove any residual soluble sulfate and NaCl. All leached carbonate powders were then reacted with an excess of 6M HCl to release the CAS from the calcite lattice, and centrifuged and filtered immediately to minimize the possibility of oxidation of any surviving sulfide minerals. The solution was separated from the insoluble residues through syringe filters (0.25 μm : details as above). BaSO_4 was precipitated by adding 2 ml supersaturated BaCl_2 solution to the CAS leachate. The NaOCl and CAS leachates treated with BaCl_2 solution were left in sealed tubes for at least 72 hours to allow complete BaSO_4 precipitation. BaSO_4 precipitates were centrifuged and rinsed several times with ultrapure until the pH reached neutral values. Finally, the precipitates were transferred to smaller containers and dried for sulfur-isotope analysis.

3.2. Sulfur-isotope and elemental concentration analysis

Sulfur-isotope analysis was undertaken on an Elementar vario PYRO cube linked to a GV Isoprime mass spectrometer in continuous flow mode in the Cohen Geochemistry Laboratories of the School of Earth and Environment, University of Leeds. 0.130–0.220 mg dried BaSO_4 powders were weighed and packed into tin cups, and flash-combusted at 1150 $^\circ\text{C}$ in the presence of pure research-grade O_2 and helium carrier gas to produce SO_2 . Excess O_2 was consumed by reaction with copper wires at 850 $^\circ\text{C}$ and water was removed by a Sicapent trap. Subsequently, SO_2 was separated from other gases using a temperature-controlled trap and purge column. Results were calibrated to the Vienna-Canyon Diablo Troilite (V-CDT) using a seawater laboratory standard (SWS-3) and a chalcopyrite inter-lab standard (CP1) assigned values of +20.3‰ and –4.56‰, respectively. These materials were in turn calibrated using the international standards (assigned values in brackets) NBS-127 (+20.3‰), NBS-123 (+17.01‰), IAEA S-1 (–0.30‰) and IAEA S-3 (–32.06‰). The repeated analysis of all laboratory standards gives a precision of $\pm 0.3\text{‰}$ (1 sd) or better.

Major-element concentrations (Ca, Mg, Mn, Sr and S) were analyzed in an aliquot of the HCl-leachate (taken prior to adding BaCl_2), using a Thermo Fisher iCAP 7400 radial Inductively Coupled Plasma Optical Emission Spectrometer (ICP-OES), also at Leeds. The analytical precision was better than 3% for all elements.

3.3. Age model and sedimentation rates

A key component of understanding the sulfur cycle is estimating the rate of isotopic change. This process requires an estimate of the age of each sample to calculate the $d\delta^{34}\text{S}_{\text{CAS}}/dt$ for the studied interval. To date, the Sinemurian–Pliensbachian and Pliensbachian–Toarcian boundary age tie-points have been well constrained through astrochronological calibration at $\sim 192.5 \pm 0.4$ Ma and $\sim 183.7 \pm 0.5$ Ma, respectively, and thus the duration of the entire Pliensbachian estimated at ~ 8.8 Myr (Huang and Hesselbo, 2014; Ruhl et al., 2016; Storm et al., 2020). Based on the biostratigraphical constraints, carbon-isotope chemostratigraphic correlation, and onset of the T-OAE negative CIE at ~ 217 m (Han et al., 2018, 2021), these two numerical age tie-points were positioned at the Sinemurian–Pliensbachian boundary (~ 61 m) and Pliensbachian–Toarcian boundary (~ 208 m) in Wölong, respectively (Fig. 6). The available astrochronological time-scale from Ruhl et al. (2016) allows for a constraint of ~ 4.2 Myr from the Sinemurian–Pliensbachian boundary to the upper SPBE boundary, so that the time duration from the upper SPBE boundary to the Pliensbachian–Toarcian boundary can be calculated as ~ 4.6 Myr (Fig. 6). Additionally, there are a number of estimates for the duration of the T-OAE negative CIE from ~ 300 to 900 kyr (e.g. Suan et al., 2008; Boulila et al., 2014; Huang and Hesselbo, 2014). However, the duration of ~ 900 kyr for the T-OAE negative CIE was employed in this study based on the data from the global stratotype section and point (GSSP) of Peniche, Portugal, because it has well-constrained biostratigraphy and a high-resolution carbon-isotope record (Hesselbo et al., 2007; Suan et al., 2008; Huang and Hesselbo, 2014; Bordalo Da Rocha et al., 2016). In the Tethys Himalaya succession, the upper SPBE and lower T-OAE CIE boundaries are located at the transition between the Zhamure and Pupuga Formations and at a more abrupt contact between the Pupuga and Nienixiongla Formations, respectively. These three formations represent different depositional environments and, assuming constant sedimentation rates for each dominant facies, the accumulation rate was estimated to be ~ 1.7 , ~ 1.7 and ~ 3.4 cm/kyr for the Zhamure, Pupuga and Nienixiongla Formations, respectively. Age uncertainties for the Sinemurian–Pliensbachian and Pliensbachian–Toarcian boundaries can be used to calculate the uncertainty on the sedimentation rate for the Pupugua Formation producing a value of ± 0.3 cm/kyr.

4. Results

4.1. Sulfur isotopes

Values of $\delta^{34}\text{S}_{\text{CAS}}$ range between +13 and +27‰ with an average of +20.3‰ (Figs. 2 and 3). In the pre-SPBE interval (~ 0 –54 m), $\delta^{34}\text{S}_{\text{CAS}}$ maintains relatively stable values around 20‰. Over the SPBE interval, an overall ~ 5 ‰ positive sulfur-isotope excursion (PSIE1) is observed between 54 and 146 m (Figs. 2 and 3), coincident with a negative shift in carbonate $\delta^{13}\text{C}$ (SPBE). Following this, and around the level of the ME, $\delta^{34}\text{S}_{\text{CAS}}$ exhibits a sharp negative–positive couplet (NSIE) over intervals of ~ 146 –167 m and ~ 167 –182 m, reaching the most extreme negative $\delta^{34}\text{S}_{\text{CAS}}$ values (~ 13 –14‰) of the measured interval, unlike the uppermost Pliensbachian–lowest Toarcian (~ 182 –218 m) that has stable values with an average of +20.9‰.

The sulfur-isotope values of NaOCl leachates ($\delta^{34}\text{S}_{\text{bleach}}$) during the CAS extraction (see section 3.1) were also analyzed, as shown in the supplementary data. $\delta^{34}\text{S}_{\text{bleach}}$ values vary between -30 to +10‰ with an overall average of -3.8 ‰ (Fig. 2). In the Sinemurian, $\delta^{34}\text{S}_{\text{bleach}}$ is quite variable with an average value of around -20 ‰. There were no $\delta^{34}\text{S}_{\text{bleach}}$ data obtained from the

stratigraphically higher interval (~ 61 –124 m) roughly corresponding to the SPBE due to low recoveries of BaSO₄. Following this missing interval, $\delta^{34}\text{S}_{\text{bleach}}$ values become noticeably more positive (~ 125 –153 m, with an average of -8.1 ‰) and reach a stable plateau (~ 164 –208 m, with an average of +6.4‰) in the upper Pliensbachian. The lowest Toarcian (~ 212 –218 m) is marked by a change to slightly more negative values fluctuating around an average of -5.6 ‰.

4.2. Elemental concentration

The CAS-sulfur content in the Wölong section is low, ranging from 4 to 130 ppm with an average value of ~ 17.6 ppm (Fig. 4). Carbonate Mg/Ca (w/w) and Mn/Sr (w/w) ratios range from 0.005 to 0.400 and 0.1 to 1.8, and have average values of 0.03 and 0.48, respectively.

5. Discussion

5.1. Preservation and diagenetic assessment of sulfur-isotope records

Although bulk $\delta^{34}\text{S}$ of carbonate-associated sulfate (CAS) is generally considered to be a proxy for primary seawater sulfur-isotope composition (e.g. Lyons et al., 2004; Gill et al., 2008; Fichtner et al., 2017), some studies have pointed out that early diagenetic alteration and dolomitization can cause significant alteration in $\delta^{34}\text{S}_{\text{CAS}}$ (Marenco et al., 2008a; Present et al., 2015). In the present study, $\delta^{34}\text{S}_{\text{CAS}}$ data display no correlation with the Mn/Sr ratio ($R^2 = 7 \times 10^{-5}$) and CAS concentrations ($R^2 = 0.03$), parameters that can be strongly influenced by diagenesis (Fig. 4A and B). The potential effect of dolomitization was tested by plotting Mg/Ca ratios against $\delta^{34}\text{S}_{\text{CAS}}$. In general, Mg/Ca ratios are low (< 0.05) and show no correlation with $\delta^{34}\text{S}_{\text{CAS}}$ ($R^2 = 0.04$; Fig. 4C). However, the correlations given above can only evaluate the likely overall effects of a diagenetic process, rather than identifying specific suspect data points; the values that plot well away from those stratigraphically adjacent need to be evaluated individually. Three samples show visible dolomitization in thin-section (5.5, 9, and 29 m), and display relatively high Mg/Ca ratios (> 0.3); the $\delta^{34}\text{S}_{\text{CAS}}$ values of these samples do not appear to be offset with respect to those of adjacent non-dolomitized samples (Fig. 2 and 4C), suggesting that dolomitization has had a negligible effect on $\delta^{34}\text{S}_{\text{CAS}}$ in this study.

Some studies have indicated that different carbonate components can carry CAS isotope signals affected by diagenetic processes, raising the possibility of a facies control on bulk CAS isotopic composition (Present et al., 2015). The studied section was characterized by shallow-water environments in the Early Jurassic and gradually evolved from mixed carbonate-siliciclastic deposits to carbonates around the boundary between the Zhamure (Sinemurian) and Pupuga (Pliensbachian) Formations (Han et al., 2016, 2021). These changes in lithofacies do not correspond to simple unidirectional shifts in $\delta^{34}\text{S}_{\text{CAS}}$ and none of the major changes during intervals of positive PSIE1, NSIE and PSIE2 corresponds with changes in lithology. Additionally, $\delta^{34}\text{S}$ values were obtained from five characteristic microfacies, each of which has a wide range of $\delta^{34}\text{S}$ values (Fig. 2). Notably, the $\delta^{34}\text{S}_{\text{CAS}}$ data (~ 20 ‰) in the upper Sinemurian of Wölong are also very close to those recorded in evaporites (~ 18 –19‰) from the Sinemurian Lias Salt, Spain (Utrilla et al., 1992; Fig. 8). The exception to the thrust of the discussion above is one sample at ~ 161 m that has a $\delta^{34}\text{S}_{\text{CAS}}$ value that is positively offset (> 10 ‰; Fig. 2) from its stratigraphically adjacent data points and has likely been affected by the addition of MSR-altered sulfate during early diagenesis under more closed-system conditions. An early diagenetic overprint is supported by the observation that bivalves and foraminifers of this sample have been filled with blocky calcite and lack evidence of compaction.

Wölong and Yunjia, southern Tibet

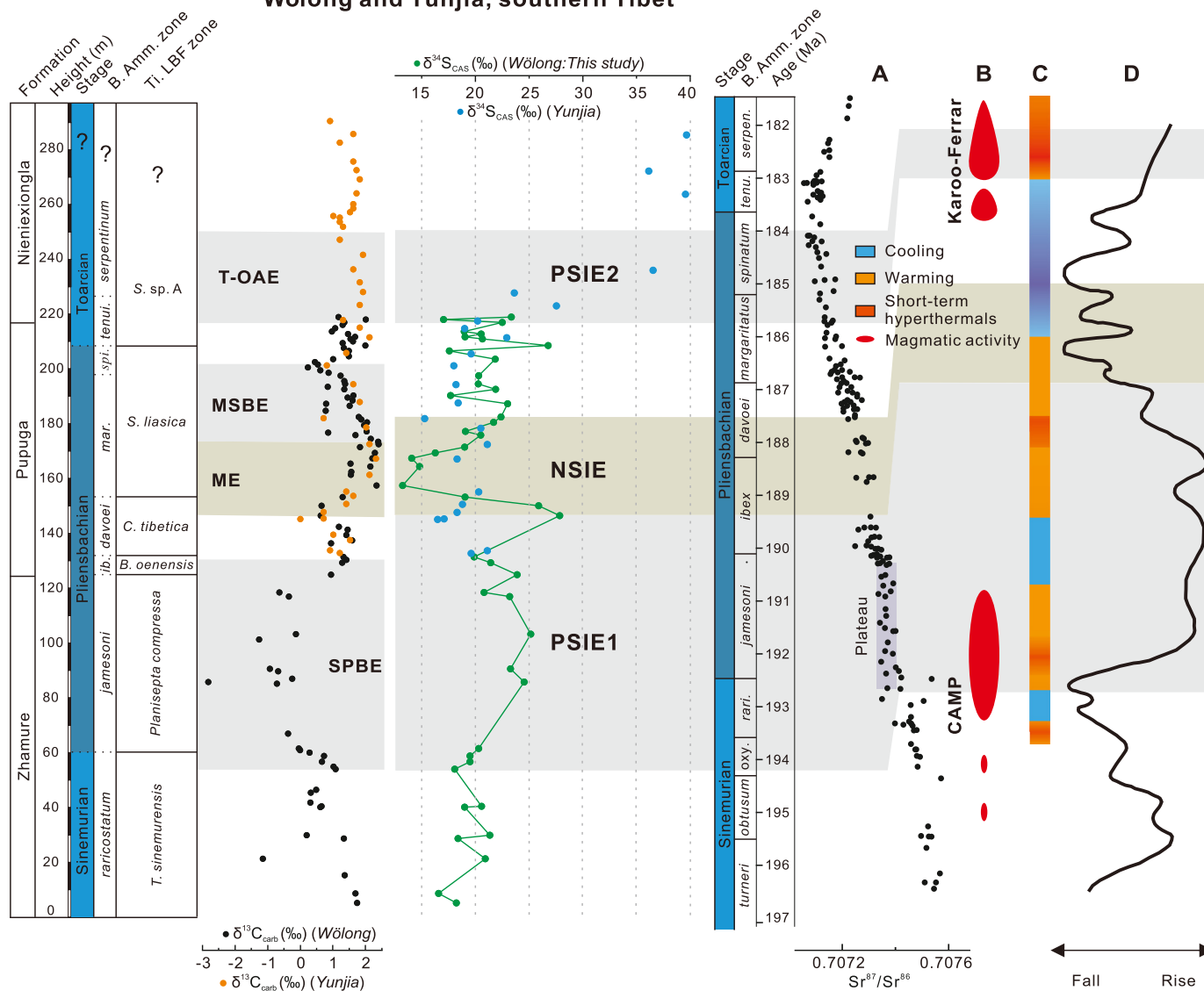


Fig. 3. Correlation between the Tibetan carbon- and sulfur-isotope data and paleoenvironmental, magmatic events and sea-level changes in the Early Jurassic. Note that the carbon- and sulfur- isotope data from Wölong and Yunjia can be combined into one composite curve based on similar trends. Time scale is based on the newly updated data of Storm et al. (2020); $^{87}\text{Sr}/^{86}\text{Sr}$ (A) is from Jones et al. (1994) and Jenkyns et al. (2002), indicating a plateau (light purple rectangle) at the base of the Pliensbachian, broadly corresponding to the SPBE and late phase of CAMP magmatic activity (B); palaeotemperature (C) and sea-level changes (D) are modified from the compiled data of Ruhl et al. (2016), Storm et al. (2020), and Hesselbo and Jenkyns (1998), respectively. Abbreviations: CAMP = Central Atlantic Magmatic Province.

In this case, sulfate consumption by MSR was likely faster than replenishment from the overlying water column, which increased the $\delta^{34}\text{S}$ of porewater sulfate (cf. Richardson et al., 2019). This suspect data point has been omitted from the trend line in Fig. 3 and from the discussion on the isotopic evolution of seawater given below. These observations suggest that, for the great majority of the samples, diagenesis and facies changes have had only minimal impact on the primary $\delta^{34}\text{S}_{\text{CAS}}$ values.

It is also possible to alter $\delta^{34}\text{S}_{\text{CAS}}$ during extraction by the addition of non-CAS sulfur phases (organic sulfur, sulfide and sulfate minerals) (Marenco et al., 2008b; Wotte et al., 2012). Whilst our extraction procedure includes thorough NaOCl bleaching and NaCl rinsing steps before CAS extraction to minimize potential experimental contamination (see section 3.1), the $\delta^{34}\text{S}_{\text{bleach}}$ is also measured to estimate the potential for this combined pool of contaminant-S to affect the CAS isotopic composition (Newton et al., 2011). The $\delta^{34}\text{S}_{\text{bleach}}$ values exhibit much more negative values than those of their paired CAS data, with pyrite-like $\delta^{34}\text{S}$ compo-

sitions, and show no correlation with $\delta^{34}\text{S}_{\text{CAS}}$ ($R^2 = 0.08$; Fig. 4D). One sample at ~ 61 m has a $\delta^{34}\text{S}_{\text{CAS}}$ value that is negatively offset from its stratigraphically adjacent data points by $>10\%$ and has a $\delta^{34}\text{S}_{\text{bleach}}$ value of nearly -30% , the most negative of the data set. These observations suggest that it has been affected by the addition of ^{34}S -depleted reduced-S either during diagenesis or extraction. This data point has also been excluded both from the trend illustrated in Fig. 3 and the later discussion on the isotopic evolution of seawater. Additionally, microfacies analysis of all analyzed carbonate samples shows that visible pyrite is rare and TOC is low, limiting the amount of contaminant-S available (Newton et al., 2011; Han et al., 2016). These observations suggest that reduced sulfur phases with $\delta^{34}\text{S}$ -depleted values are low in concentration and effectively removed, meaning that the effect of contamination during extraction on $\delta^{34}\text{S}_{\text{CAS}}$ is negligible.

In summary, the $\delta^{34}\text{S}_{\text{CAS}}$ data appear to show only limited influence from diagenesis, facies and reduced sulfur oxidation, and

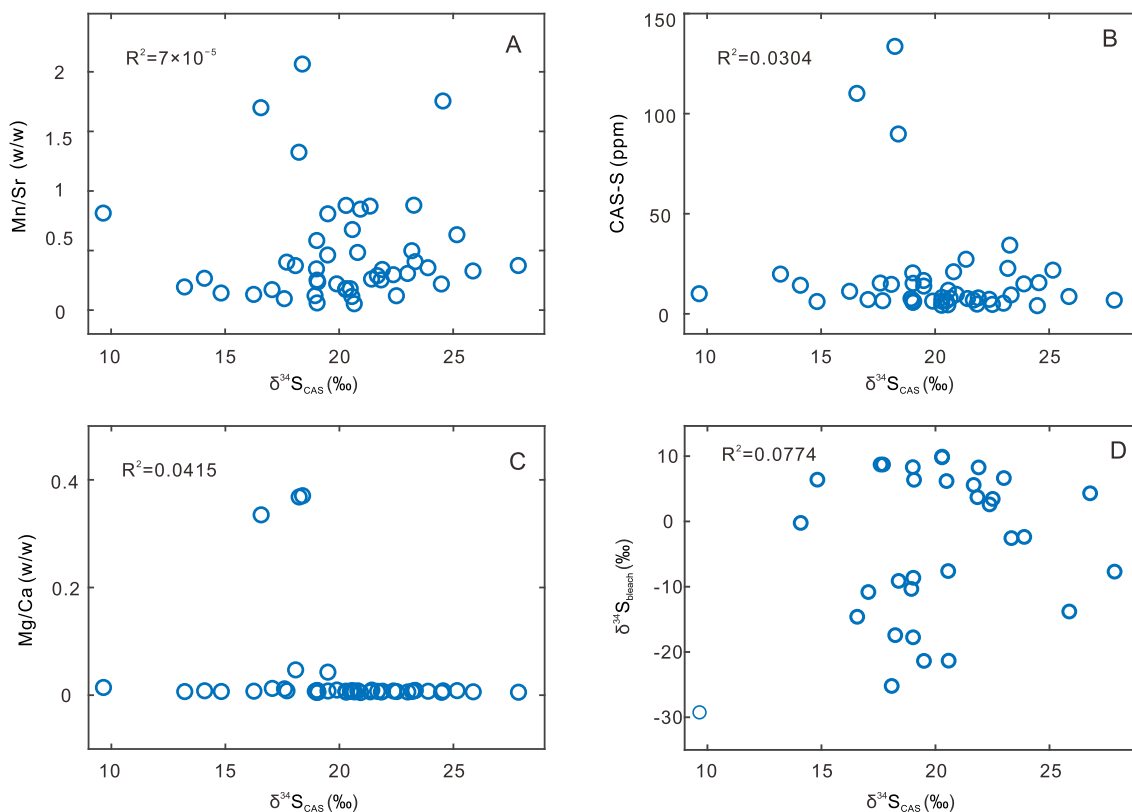


Fig. 4. Evaluation of possible diagenetic alteration of $\delta^{34}\text{S}_{\text{CAS}}$ values. Cross-plots of $\delta^{34}\text{S}_{\text{CAS}}$ against elemental concentrations. A. $\delta^{34}\text{S}_{\text{CAS}}$ (‰)–Mn/Sr (w/w) ($R^2 = 7 \times 10^{-5}$), B. $\delta^{34}\text{S}_{\text{CAS}}$ (‰)–[CAS] (ppm) ($R^2 = 0.0304$), C. $\delta^{34}\text{S}_{\text{CAS}}$ (‰)–Mg/Ca (w/w) ($R^2 = 0.0415$), D. $\delta^{34}\text{S}_{\text{CAS}}$ (‰)– $\delta^{34}\text{S}_{\text{bleach}}$ (‰) ($R^2 = 0.0774$).

thus can be interpreted as primary changes in the isotopic composition of at least regional seawater sulfate.

5.2. Long-term sulfur-isotope perturbations in the Early Jurassic and the regulation of atmospheric oxygen

Ample sedimentary evidence has suggested that the Jurassic Tethys Himalaya was located within a narrow linear zone on the northern margin of the Indian continent (peri-continental sea, e.g. Han et al., 2021 and references therein). Our studied section was formerly situated at the southern part of the linear zone, directly facing the open Tethys Ocean (Fig. 1, see section 2). The Lower Jurassic larger benthic foraminifera and *Lithiotis* Fauna of the Tibetan Tethys Himalaya are similar to those found in the western Tethys (Jadoul et al., 1998; Wignall et al., 2006; Han et al., 2016, 2018, 2021), indicating that no significant geographic barrier existed between the eastern and western Tethys. Our screened Tibetan $\delta^{34}\text{S}_{\text{CAS}}$ record therefore likely reflects primary isotopic changes in the ocean sulfate reservoir during the Early Jurassic at this location.

The paired carbonate carbon and CAS sulfur-isotope records have a weak negative correlation (Fig. 5), with an almost identical slope to that derived from evaporite and carbonate records across the whole Phanerozoic (Veizer et al., 1980). Since the burial of reduced carbon and sulfur regulates the production of atmospheric oxygen, this negative correlation potentially implies that its gaseous concentration remained near-constant across this interval (Veizer et al., 1980). However, this finding is in contrast to data from the lower Paleozoic and upper Mesozoic where sulfate-sulfur and carbonate-carbon isotopic records are positively correlated, implying pulsed oxygen fluxes to the atmosphere (Gill et al., 2011b; Owens et al., 2013; He et al., 2019; Bowman et al., 2019). This situation was likely interrupted by the enhanced burial

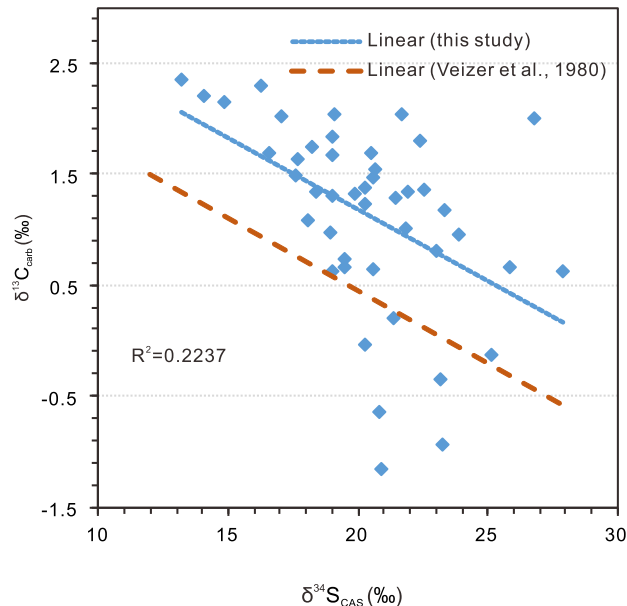


Fig. 5. The correlation between carbonate carbon and CAS-sulfur isotopes ($R^2 = 0.2237$).

of organic carbon and pyrite which would have induced a pulse in atmospheric O_2 during the T-OAE (e.g. Garrels and Lerman, 1984; Berner, 2006) and ultimately may have terminated this OAE, as indicated by charcoal records (Baker et al., 2017).

5.2.1. Late Sinemurian–early Pliensbachian

In general, the lower section shows an overall positive $\delta^{34}\text{S}_{\text{CAS}}$ excursion (PSIE1, ~54 m to 146 m), generally in phase with the CIE

of the SPBE. This CIE has been linked to increased flux of isotopically light carbon into the ocean–atmosphere system as a result of the late eruption pulses of the Central Atlantic Magmatic Province and/or hydrothermal activity connected to the break-up of Pangaea (Fig. 3; Ruhl et al., 2016; Price et al., 2016; Franceschi et al., 2019; Han et al., 2021). This net increase in volcanic degassing could have triggered global warming, as supported by a negative excursion in $\delta^{18}\text{O}_{\text{carb}}$ starting at the earliest *jamesoni* zone and culminating in the *davoei* zone in the early Pliensbachian in both western Tethyan and northern European regions (Jenkyns et al., 2002; Korte and Hesselbo, 2011; Price et al., 2016; Baghli et al., 2020). Global warming would have resulted in lower dissolved oxygen levels and reduced the oceans capacity for oxic degradation of organic matter. The resultant increase in the amount of organic matter available for MSR would have enhanced pyrite burial, thereby raising marine $\delta^{34}\text{S}_{\text{CAS}}$ values, since ^{32}S is preferentially utilized during MSR (Bernier, 1984). Organic sulfur could be another possible sink for reduced sulfur when pyrite formation was limited by the availability of iron (Owens et al., 2013; Raven et al., 2019).

There is sedimentological evidence of abundant organic-rich sediments of hemipelagic facies in the Lusitanian Basin, Portugal: specifically, black shales in distal settings and framboidal pyrite in proximal settings were found in the upper Sinemurian (Duarte et al., 2010; Boussaha et al., 2014). In addition, organic-rich carbonate-ramp facies are present in the Basque–Cantabrian Basin, northern Spain (Rosales et al., 2006), and in the shallow-water platform carbonates of northern Italy (Franceschi et al., 2014) during the SPBE. Relative enrichment in organic matter is also seen around the Sinemurian–Pliensbachian boundary in the stratigraphically expanded Lower Jurassic Mochras core from Wales (Storm et al., 2020). These observations suggest that, at least in the European area, the SPBE interval may have been favorable for an increase in productivity and/or preservation of organic matter. Furthermore, black siliceous radiolarian-rich sediments of the late Sinemurian–early Pliensbachian age are known from exotic terrains in the Koryak–Western Kamchatka Orogenic Belt, East Asia (Filatova et al., 2020). These sediments derive from the palaeo-Pacific Ocean and point to this now-vanished area as a major sink for organic matter at various times during the Jurassic. That the carbon-isotope records do not reflect the enhanced global production and burial of organic matter most likely indicates the release of more isotopically negative volcanogenic carbon dioxide that counterbalanced the effects of organic-matter burial that would otherwise have produced a positive CIE.

An alternative explanation of the positive $\delta^{34}\text{S}_{\text{CAS}}$ shift relates to sea-level rise. Most pyrite burial occurs on the continental shelves, so during sea-level highstands the shelf area expands and pyrite burial increases, whereas during sea-level lowstands, the shelf area contracts and previously buried pyrite is oxidized (Turchyn and Schrag, 2006; Markovic et al., 2015). A significant transgression at the beginning of the SPBE, possibly related to global warming, is widely documented in the Boreal and Tethyan regions, as well as in southeastern Panthalassa (Fig. 3; Hesselbo and Jenkyns, 1998; Korte and Hesselbo, 2011), and this may have provided increased accommodation space for pyrite burial. However, such a process would equally have provided accommodation for enhanced organic-carbon burial, because the vast majority of such material is buried on continental shelves (Bernier, 1982). Although sea-level rise and expansion of continental shelves may have played an additional role in global organic-carbon burial, it manifestly was not sufficient to reverse the effects of volcanogenic carbon release that ultimately caused a negative CIE during the SPBE.

Reduced sulfate weathering fluxes with $\delta^{34}\text{S}$ -depleted values also have the potential to cause this positive $\delta^{34}\text{S}_{\text{CAS}}$ shift. However, enhanced temperature and elevated CO_2 concentration

are more likely to have increased chemical weathering of the ocean floor and on continents. Increased weathering fluxes have been suggested as an explanation for the $^{87}\text{Sr}/^{86}\text{Sr}$ plateau in the *jamesoni* zone of the Pliensbachian as a counterpoint to the longer term unradiogenic marine hydrothermal/basalt strontium flux (Fig. 3; Ruhl et al., 2016). Whilst it might be expected that any such weathering increase would also have enhanced the ^{34}S -depleted riverine sulfate flux into the ocean, the positive isotopic excursion in CAS record suggests any such affect was small relative to increased pyrite burial caused by warming and/or sea-level rise.

5.2.2. Late Pliensbachian

Following the SPBE, an overarching negative shift in $^{34}\text{S}_{\text{CAS}}$ (NSIE; ~144–182 m; Fig. 3) corresponds stratigraphically with the positive CIE dated to the *margaritatus* zone (ME). The ME positive CIE has been suggested to link to an enhanced organic-carbon burial event due to the expansion of oceanic oxygen-depleted conditions on a global scale (e.g. Suan et al., 2010; Korte and Hesselbo, 2011; Silva and Duarte, 2015; Ruhl et al., 2016; De Lena et al., 2019). Such conditions typically would have favored increased pyrite burial, consequently forcing the $\delta^{34}\text{S}$ of seawater sulfate to more positive values. However, the early phase of the ME is accompanied by a pronounced negative excursion in $\delta^{34}\text{S}_{\text{CAS}}$ (~146–167 m; Fig. 3). This shift to lower values could be explained by the late Pliensbachian cooling and sea-level fall suggested by many authors (Fig. 2; e.g. Hesselbo and Jenkyns, 1998; Suan et al., 2010; Korte and Hesselbo, 2011; Korte et al., 2015; Baghli et al., 2020). During this time interval, newly exposed shelf sediments would have been weathered and reduced sulfur oxidation would have become more significant, thereby increasing input of $\delta^{34}\text{S}$ -depleted sulfate to the oceans and causing this negative $\delta^{34}\text{S}_{\text{CAS}}$ excursion. However, such a mechanism is at odds with the carbon-isotope record since we would also expect organic carbon in these newly exposed sediments to be oxidized, forcing the ocean dissolved inorganic carbon (DIC) reservoir towards more negative values: the reverse of what is observed in the early phase of the ME. This phenomenon could be explained by the “weathering hypothesis” suggested by Kump et al. (1999) whereby increased weathering of vast areas of carbonate sediments during sea-level fall, rather than increased organic-carbon burial, could also drive the DIC pool to more positive $\delta^{13}\text{C}$ values. Extensive carbonate platforms were widely distributed along the tropical/subtropical Tethys margin during the Sinemurian–Pliensbachian (Han et al., 2021 and references therein), which could have easily been exposed as a result of the late Pliensbachian global sea-level fall. By contrast, during the late phase of the ME, the previous NSIE is seen to gradually decay and return to pre-NSIE values, being compatible with coupled enhanced organic-carbon and pyrite burial in marine sediments that drove both seawater carbon ($\delta^{13}\text{C}$) and sulfate ($\delta^{34}\text{S}$) to higher values.

5.3. Seawater sulfate concentrations in the Early Jurassic

We apply the “rate method” via the equations below to calculate the sulfate concentration changes in the Early Jurassic (cf. Algeo et al., 2015). This method depends on the rate of change of seawater sulfate- $\delta^{34}\text{S}$ and the difference between $\delta^{34}\text{S}_{\text{CAS}}$ and $\delta^{34}\text{S}_{\text{PY}}$ values ($\Delta^{34}\text{S}_{\text{CAS-PY}}$), which are a function of the mass of seawater sulfate (M_o). The parameters and definitions for the variables used in the equations below are detailed in Table 1. Based on Equation (1), the theoretical maximum rate of $\delta^{34}\text{S}$ change ($d\delta^{34}\text{S}_{\text{CAS}}/dt$ (max)) is reached when sulfur input to the ocean reaches zero ($F_{\text{IN}} = 0$, Equation (2)), and the standing seawater reservoir is consumed through pyrite burial. Given that the observed $d\delta^{34}\text{S}_{\text{CAS}}/dt$ (max) is always lower than the theoretical maximum rate of change, this method provides a maximum estimate of

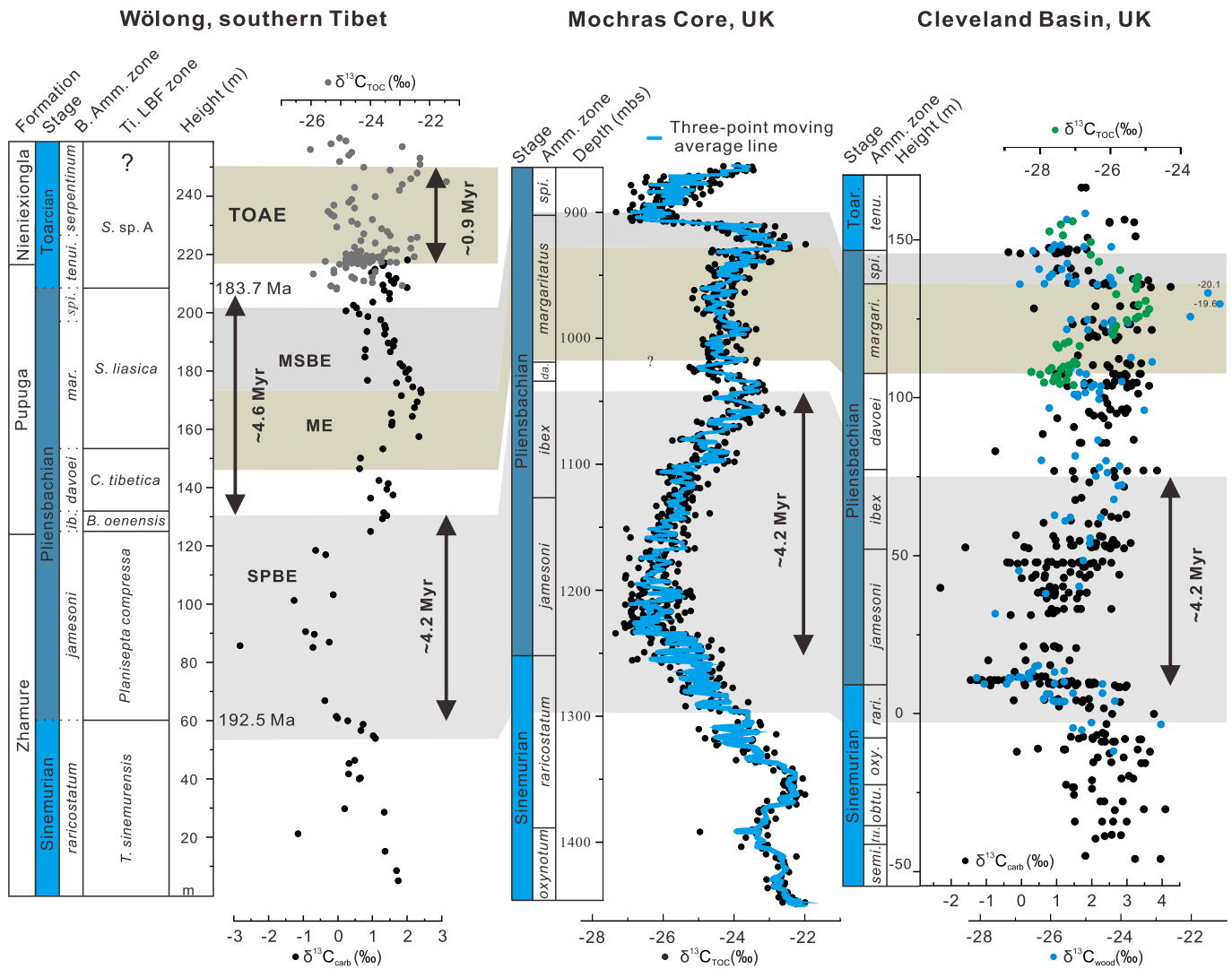


Fig. 6. Age model for the Wölong section based on carbon-isotope chemostratigraphical correlation between the Wölong (Han et al., 2018, 2021) and the reference sections of the Mochras core, Wales, UK (Storm et al., 2020) and Cleveland Basin, Yorkshire, UK (Korte and Hesselbo, 2011; Ruhl et al., 2016). The age tie-points at the Sinemurian–Pliensbachian (192.5 Ma) and Pliensbachian–Toarcian (183.7 Ma) boundaries are from Huang and Hesselbo (2014) and Storm et al. (2020), respectively. The duration of the T–OAE CIE is from Suan et al. (2008) and Huang and Hesselbo (2014).

Table 1

Values of model parameters for rate method, which are taken from Algeo et al. (2015).

Model parameter	Symbol	Rate/Value
Pyrite sink flux	F_{PY}	$4 \times 10^{13} \text{ mol yr}^{-1}$
S-isotope fractionation between CAS and pyrite	ΔS_{CAS-PY}	40‰
Observed rate of variation in $\delta^{34}S_{CAS}$	$d\delta^{34}S_{CAS}/dt$	Calculated in experiments
Seawater sulfate concentrations	$[SO_4^{2-}]$	Predicted from model
Unit-conversion constant	$k1$	1×10^6
Constant relating to the mass of seawater sulfate	$k2$	$2.22 \times 10^{-20} \text{ mMg}^{-1}$

seawater sulfate concentrations (Equation (3)). These estimates are most meaningful where rates of change are highest in the $\delta^{34}S_{CAS}$ record.

$$d\delta^{34}S_{CAS}/dt = (F_{IN} \times \Delta^{34}S_{IN-SW} - F_{PY} \times \Delta^{34}S_{CAS-PY})/M_0 \quad (1)$$

$$d\delta^{34}S_{CAS}/dt(\text{max}) = (F_{PY} \times \Delta^{34}S_{CAS-PY})/M_0 \quad (2)$$

$$[SO_4^{2-}] = k1 \times k2 \times M_0 \quad (3)$$

Based on the age tie-points of the Sinemurian–Pliensbachian and Pliensbachian–Toarcian boundaries, and sedimentation rates of each dominant facies obtained in section 3.3, the age of each

sample and time interval between samples can be obtained (see Supplementary material). The average calculated time interval between stratigraphically adjacent samples in our study is 0.29 Myr, with 81% of samples having an interval ≤ 0.4 Myr. Therefore, data-smoothing grids of 0.1 Myr, 0.25 Myr and 0.4 Myr were used to derive $\delta^{34}S_{CAS}$ input curves (Fig. 7). Note that we have included Toarcian data of Newton et al. (2011) from the nearby Yunjia section, which is readily correlatable to the outcrop documented here (Wölong section, ~ 500 m away from Yunjia) and used them in this isotopic study. The estimates of maximum sulfate concentration derived from all three curves show similar trends but produce a range of absolute values. Linking the lowest points on these curves

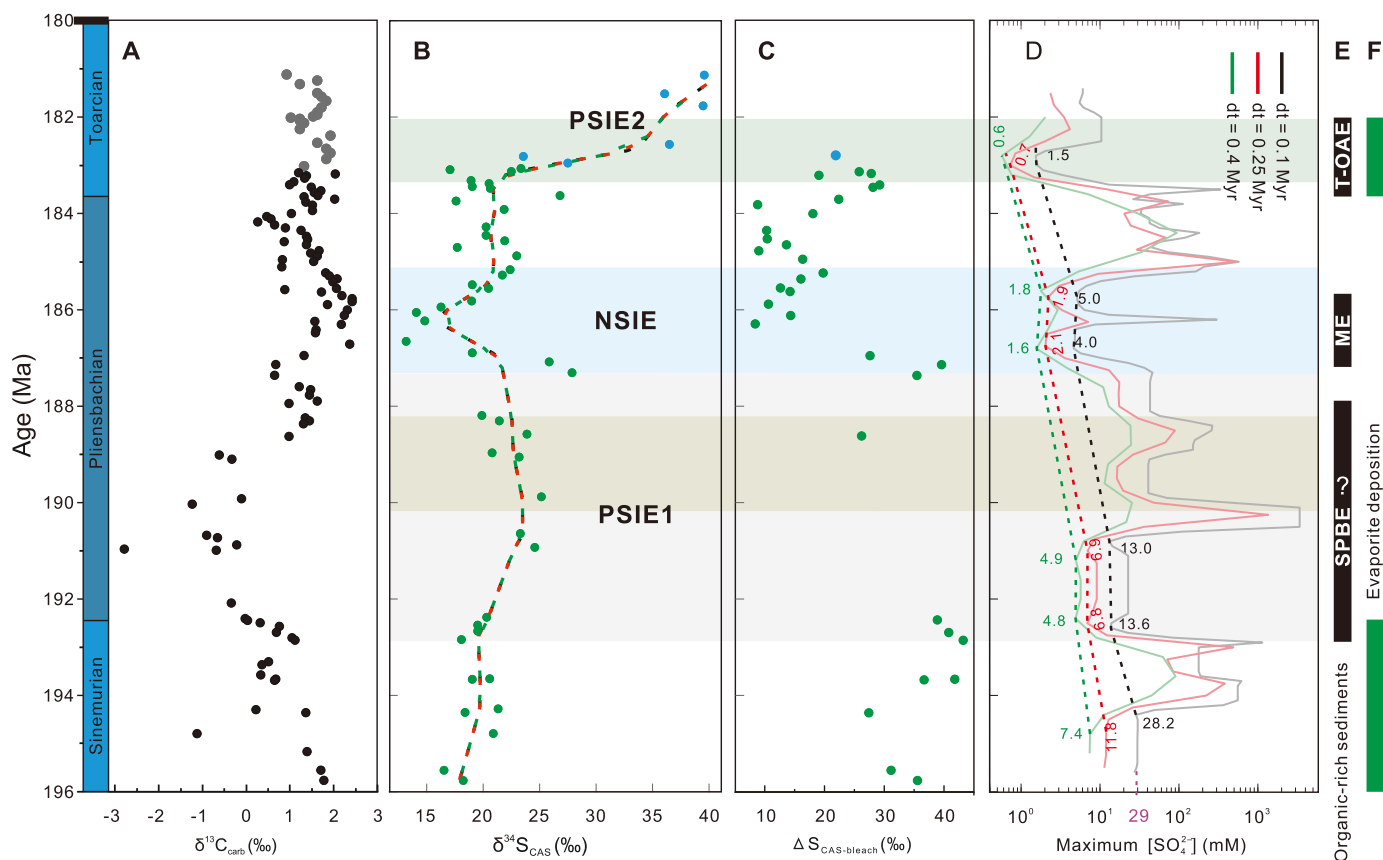


Fig. 7. $\delta^{13}\text{C}_{\text{carb}}$, $\delta^{34}\text{S}_{\text{CAS}}$ and $\Delta\text{S}_{\text{CAS-bleach}}$ data vs maximum seawater sulfate concentrations ($[\text{SO}_4^{2-}]$) in the Sinemurian–Toarcian. A: $\delta^{13}\text{C}_{\text{carb}}$ data are from Wölong (black, Han et al., 2021) and Yunjia (gray, Newton et al., 2011). B: $\delta^{34}\text{S}_{\text{CAS}}$ data are from Wölong (green, this study) and Yunjia (blue, Newton et al., 2011), and the dashed curves are the LOWESS trend (span=0.2) based on $\delta^{34}\text{S}_{\text{CAS}}$ data, with smoothing grids at 0.1 Myr (black), 0.25 Myr (red) and 0.4 Myr (green), respectively. C: $\Delta\text{S}_{\text{CAS-bleach}}$ data are from Wölong (green, this study) and Yunjia (blue, Newton et al., 2011). (D) Maximum $[\text{SO}_4^{2-}]_{\text{sw}}$ was calculated using the rate method of Algeo et al. (2015) with LOWESS-smoothed data at different grids; the corresponding dotted curve linking the lower envelope of the high-frequency maximum $[\text{SO}_4^{2-}]_{\text{sw}}$ line is expected to represent the best estimate and was marked with corresponding colors. (E) and (F): Possible processes for persistently driving down $[\text{SO}_4^{2-}]_{\text{sw}}$ in the Early Jurassic, such as the organic-rich sediment and pyrite burial in the intervals of the SPBE, ME and T-OAE, and evaporite burial in the Sinemurian to Toarcian interval. Note that the ocean sulfate concentration in the modern ocean is ~ 29 mM.

produces the most likely estimate of seawater sulfate evolution through time since these values represent the points of maximum $d\delta^{34}\text{S}_{\text{CAS}}/dt$. The resulting trends suggest that sulfate concentrations persistently declined from values of between 7.4 to 28.2 mM in the late Sinemurian to between 0.6 to 1.5 mM in the early Toarcian. However, there are uncertainties of age constraints for the Sinemurian–Pliensbachian ($\sim 192.5 \pm 0.4$ Ma, Ruhl et al., 2016) and Pliensbachian–Toarcian ($\sim 183.7 \pm 0.5$ Ma, Storm et al., 2020) boundaries. Applying these uncertainties produces maximum and minimum estimates for the duration of the Pliensbachian of 9.7 and 7.9 Myr. Additionally, the Phanerozoic enrichment factor between oceanic sulfate and sedimentary pyrite ranges from ~ 30 to $\sim 45\%$ (Algeo et al., 2015). Both the age and enrichment factor uncertainties were implemented in a sensitivity test for the sulfate concentration calculation. Changes in both age model and enrichment factor produce similar trends in the variation of sulfate concentration (see Supplementary Figs. S1 and S2).

There are relatively few estimates with which to compare our data. He et al. (2020) calculate that sulfate concentrations were < 1 mM during the Triassic–Jurassic boundary extinction interval, so our data imply a substantial rise in sulfate concentrations during the late Hettangian–early Sinemurian. Halite fluid-inclusion data for sulfate concentration are extremely rare in the Upper Triassic and absent in the Lower Jurassic (Horita et al., 2002). Estimates derived by a similar rate of isotopic change methodologies from European CAS isotope curves are broadly consistent with the idea

of a very low sulfate ocean in the early Toarcian (~ 1 –5 mM, Newton et al., 2011; ~ 4 –8 mM, Gill et al., 2011a), but our estimates are lower because the scale of $\delta^{34}\text{S}$ change is much larger in Tibet over a similar time frame. The general conclusion of a low sulfate ocean in the late Pliensbachian and early Toarcian is also supported by the abundant occurrence of siderites at these times documented in the Cardigan Bay and Cleveland basins, UK (Sellwood, 1971; Xu et al., 2018), presumably where the local supply of reactive iron and organic carbon was sufficient. Siderite is generally produced as an early diagenetic mineral under reducing and low-sulfate conditions that provide rather limited reduced sulfur during the process of organic-matter oxidation but are favorable for the reaction between abundant reduced Fe^{2+} and CO_3^{2-} (e.g. Huggett et al., 2000).

The long-term variations in sulfate concentration estimated by the rate method are also supported by changes in the enrichment factor between our CAS and bleach isotope data ($\Delta\text{S}_{\text{CAS-bleach}}$). $\delta^{34}\text{S}_{\text{bleach}}$ is not a perfect measure of the reduced sulfur pools in the sediment as it can also extract sulfate minerals and organic sulfate, but it does provide an approximate measure of their isotopic composition since the presence of significant amounts of primary sulfate is very unlikely (Wotte et al., 2012) and our studied interval generally contains little organic carbon (Newton et al., 2011; Han et al., 2018). Although very little pyrite was identified in thin-section, small (micron-scale) framboids could be significant since they were observed in the nearby Yunjia section (Wignall

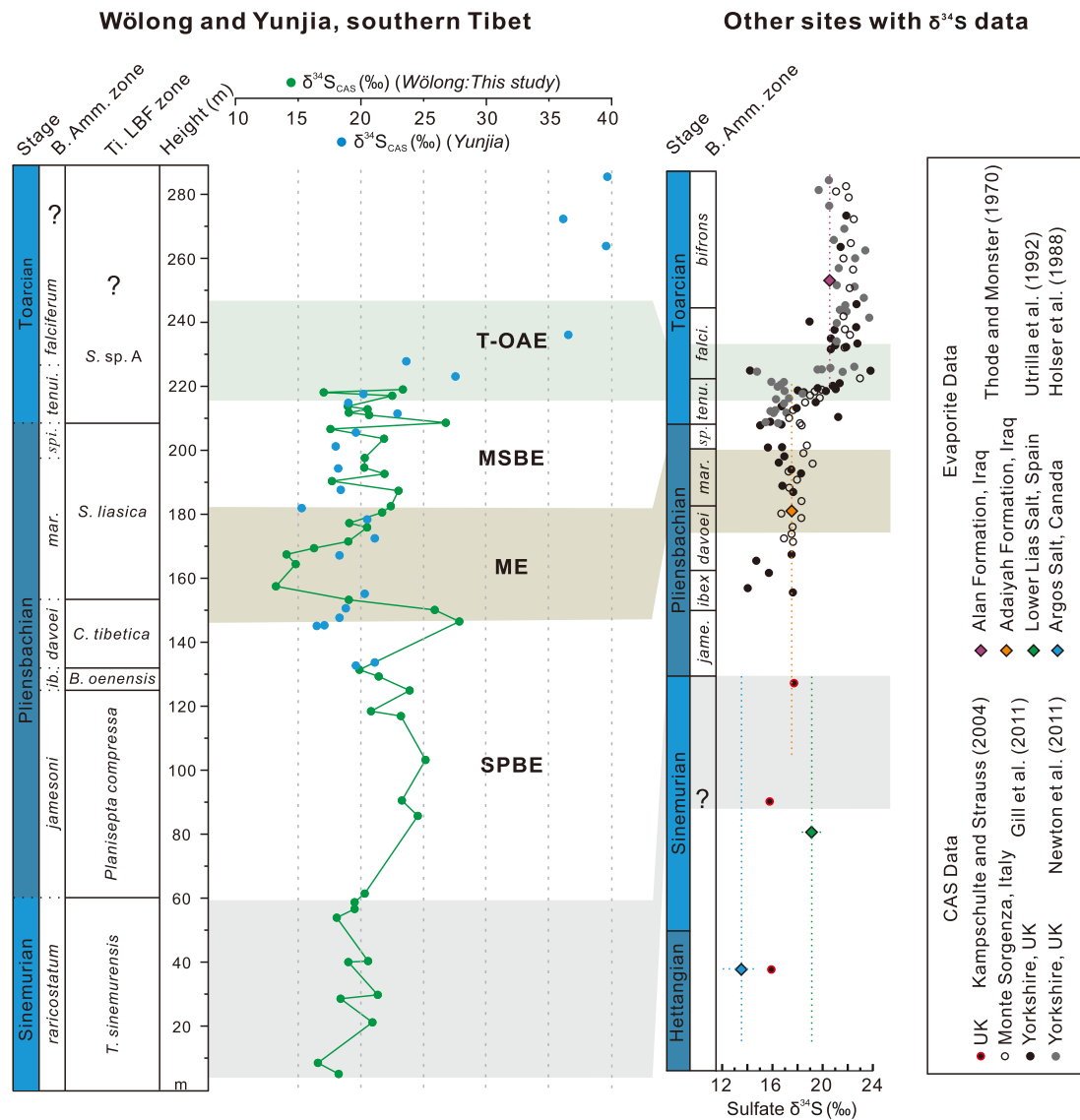


Fig. 8. $\delta^{34}\text{S}$ correlation between Wölong (green, this study) and Yunjia (blue, Newton et al., 2011) of Tibet and other sites of Early Jurassic age. $\delta^{34}\text{S}$ data of CAS are from Kampschulte and Strauss (2004) and Gill et al. (2011a), and of evaporites are from Thode and Monster (1970), Utrilla et al. (1992) and Holser et al. (1988). Bars on the evaporite data indicate estimates on depositional age and absolute value range based on the reported results.

et al., 2006). As sulfate supply becomes more limited, we expect the isotopic offset between the reduced sulfur in the sediment and seawater sulfate to decrease as a greater proportion of diffusion of supplied sulfate is converted to sulfide in the sediment (e.g. Fike et al., 2015; Sim et al., 2015). Our $\Delta\text{S}_{\text{CAS}}^{\text{bleach}}$ data are qualitatively consistent with the rate-method estimates of sulfate concentration: large and constant $\Delta\text{S}_{\text{CAS}}^{\text{bleach}}$ values in the upper Sinemurian and lower Pliensbachian (Fig. 7), where we calculate high sulfate concentrations, become much smaller in the upper Pliensbachian and into the lowest Toarcian, where our estimates of marine sulfate concentration are much lower.

The mechanism triggering low sulfate concentrations is likely to be linked to overall increased evaporite burial associated with the break-up of Pangaea during the Early Jurassic along the continental margins of the western Tethys and proto-Atlantic (Holser et al., 1988; Turner and Pelz, 2017). The marked increase implied by the difference between Triassic–Jurassic boundary estimates of <1 mM and our late Sinemurian estimates of 7.4–28.2 mM may be due to rapid re-dissolution of some of the previously deposited evaporite deposits during a sea-level rise in the late Hettangian–early Sinemurian, as envisaged by Holser et al. (1988) and Williford et

al. (2009). Episodes of organic-rich deposition and enhanced pyrite burial inferred from the positive $\delta^{34}\text{S}_{\text{CAS}}$ shifts during the SPBE, ME and T-OAE could have also played a significant role in the draw-down of seawater sulfate concentrations during the Sinemurian to Toarcian interval.

5.4. Comparison with other sulfur-isotope records in the Early Jurassic

When sulfate concentrations decrease to such an extent that the seawater sulfate residence time is equal to or shorter than the global average mixing time, $\delta^{34}\text{S}_{\text{CAS}}$ records are more likely to be affected by local/regional processes, and thus show different trends and values between geographically distant ocean basins (Luo et al., 2010; Newton et al., 2011; Gomes et al., 2016). By contrast, in conditions of high seawater sulfate concentrations, trends and values observed in $\delta^{34}\text{S}_{\text{CAS}}$ can have supra-regional or global expression, as is the case for the Late Cenozoic ocean when sulfate concentrations were high (~ 29 mM), and $\delta^{34}\text{S}_{\text{CAS}}$ records are globally homogeneous (Yao et al., 2019). Therefore, a global comparison of $\delta^{34}\text{S}$ values can provide qualitative information as to how the sulfate concentrations impacted the sulfur cycle.

The $\delta^{34}\text{S}_{\text{CAS}}$ measured in this study shows relatively stable values ($19.3 \pm 1.44\%$, $n=11$) for the upper Sinemurian (~ 0 –60 m), broadly in agreement with the results of several evaporite (Spain) and CAS (UK) data points showing 18–19‰ and 16–18‰, respectively, in the Hettangian–Sinemurian (Fig. 8; Utrilla et al., 1992; Kampschulte and Strauss, 2004). Our estimates of relatively high sulfate concentration at this time (Figs. 7 and 8) are consistent with a relatively isotopically homogenous ocean.

There are generally large differences between our Tibetan records and those from elsewhere in the subsequent Pliensbachian to Toarcian interval, although there are no comparable data for the *Jamesoni* zone (Fig. 8). Tibetan $\delta^{34}\text{S}_{\text{CAS}}$ tends to be more positive than European data in this interval, except for the short-term plateau with lower $\delta^{34}\text{S}_{\text{CAS}}$ (~ 157 –167 m) in the upper Pliensbachian. The T-OAE interval is characterized by positive excursions in both Europe and Tibet although the magnitude in the latter is far larger than in northern and southern (Tethyan) Europe ($\sim +20\%$ vs $\sim +6\%$; Gill et al., 2011a; Newton et al., 2011). These observations may suggest that the initial formation of an isotopically heterogeneous ocean for seawater sulfate began in the Pliensbachian as concentrations began to fall, culminating in a very different scale of response between the European epicontinental sea and western Tethyan continental margin, where coeval isotopic values are comparable, and the more remote easterly Tibetan shelf at the time of expanded early Toarcian anoxia (Figs. 7 and 8).

The Early Jurassic, particularly the Pliensbachian to Toarcian interval, was therefore likely characterized by frequent sulfur-isotope perturbations in seawater sulfate in a similar way to the carbon-isotope system. Consequently, the pattern of regional change in sulfate isotopes was likely a function of declining seawater sulfate concentrations, potentially resulting in substantial regional differences. The two significant perturbations in the SPBE and ME observed in Tibetan sections have not been reported elsewhere, either due to the extremely limited high-resolution $\delta^{34}\text{S}$ data from the Lower Jurassic (pre-Toarcian) currently available or because these perturbations are regional in nature. It is thus necessary to seek additional coeval CAS- $\delta^{34}\text{S}$ data from other regions to confirm the global significance and spatial evolution of the Early Jurassic sulfur cycle.

6. Conclusions

In this study, we present new $\delta^{34}\text{S}_{\text{CAS}}$ from the Lower Jurassic (Sinemurian–Pliensbachian) carbonate platform in the Tibetan Himalaya. Combined with the existing $\delta^{34}\text{S}_{\text{CAS}}$ data of the lower Toarcian from this region, the long-term sulfur-isotope cycle for much of Early Jurassic time has been reconstructed. The Sinemurian–Pliensbachian boundary event (SPBE) is characterized by a $\sim +5\%$ excursion in $\delta^{34}\text{S}_{\text{CAS}}$ coincident with the globally developed negative CIE and can be explained by enhanced pyrite and organic-sulfur burial in the global ocean. A negative $\delta^{34}\text{S}_{\text{CAS}}$ shift contemporaneous with the early phase of the positive CIE of the late Pliensbachian event (ME) is interpreted as reflecting increased $\delta^{34}\text{S}$ -depleted sulfate input related to the increased weathering fluxes of sulfate. Subsequently, a positive shift in the sulfur-isotope curve in the late phase of the ME was likely fostered by persistent $\delta^{32}\text{S}$ -rich pyrite burial.

Modeling of the sulfur cycle shows that the oceanic sulfate concentrations steadily declined during the Sinemurian–Toarcian interval, reaching their lowest values in the early Toarcian. The estimated values are all lower than those of the modern ocean (~ 29 mM), suggesting a relatively small sulfate reservoir around that time in the Jurassic. This progressively decreasing sulfate reservoir could be attributed to widespread evaporite burial in the southern margins of the Tethys, supplemented by enhanced pyrite burial during the SPBE, ME and T-OAE. Our results show that sul-

fate concentrations may still have been high enough to maintain a sulfur-isotope homogeneous ocean in the late Sinemurian. However, a persistent decrease in sulfate concentrations was likely to have caused spatial heterogeneity in marine sulfur-isotope records from the beginning of the Pliensbachian, culminating in a greatly amplified response to the T-OAE in Tibet when compared to northern and southern Europe.

CRedit authorship contribution statement

Zhong Han performed writing, original draft and conceptualization. Xiumian Hu performed writing, review, editing and conceptualization. Tianchen He, Robert J. Newton, Hugh C. Jenkyns, Robert A. Jamieson, Marco Franceschi performed writing, review and editing.

Declaration of competing interest

The authors declare that they have no known competing financial interests or personal relationships that could have appeared to influence the work reported in this paper.

Acknowledgements

We are grateful for the help of Dr Andrew Hobson and Dr Stephen Reid in the Cohen Laboratories, University of Leeds, for their analytical and technical support. We thank Wei An, Juan Li and Shiyi Li for their assistance in the field, and Yiwei Xu, Weiwei Xue, and Wei Li for their help in the laboratory. This study was supported by the National Natural Science Foundation of China (grant numbers: 41888101, 42002121, 41525007), scholarship grant from China Scholarship Council (201706190163), and the Program B (201802B079) for Outstanding PhD student and research grant (2021-LAMD-K03) from the State Key Laboratory of Mineral Deposit Research of Nanjing University. RJN and TH were supported by the Natural Environment Research Council grant number NE/N018559/1. We are further grateful for the constructive reviews from Genming Luo, Charles Diamond, Benjamin Gill, and the editorial guidance from Timothy Lyons. This manuscript is a contribution to the IGCP 739 and Integrated Understanding of the Early Jurassic Earth System.

Appendix A. Supplementary material

Supplementary material related to this article can be found online at <https://doi.org/10.1016/j.epsl.2021.117261>.

References

- Algeo, T.J., Luo, G.M., Song, H.Y., Lyons, T.W., Canfield, D.E., 2015. Reconstruction of secular variation in seawater sulfate concentrations. *Biogeosciences* 12, 2131–2151.
- Baghli, H., Mattioli, E., Spangenberg, J., Bensalah, M., Arnaud-Godet, F., Pittet, B., Suan, G., 2020. Early Jurassic climatic trends in the South-Tethyan margin. *Gondwana Res.* 77, 67–81.
- Baker, S.J., Hesselbo, S.P., Lenton, T.M., Duarte, L.V., Belcher, C.M., 2017. Charcoal evidence that rising atmospheric oxygen terminated Early Jurassic ocean anoxia. *Nat. Commun.* 8, 15018.
- Berner, R.A., 1982. Burial of organic carbon and pyrite sulfur in the modern ocean: its geochemical and environmental significance. *Am. J. Sci.* 282, 451–473.
- Berner, R.A., 1984. Sedimentary pyrite formation: an update. *Geochim. Cosmochim. Acta* 48, 605–615.
- Berner, R.A., 2006. GEOCARBSULF: a combined model for Phanerozoic atmospheric O_2 and CO_2 . *Geochim. Cosmochim. Acta* 70, 5653–5664.
- Blackburn, T.J., Olsen, P.E., Bowring, S.A., McLean, N.M., Kent, D.V., Puffer, J., McHone, G., Rasbury, E.T., Et-Touhami, M., 2013. Zircon U–Pb geochronology links the end-Triassic extinction with the central Atlantic magmatic province. *Science* 340, 941–945.

- Bordalo Da Rocha, R., Mattioli, E., Duarte, Vítor L., Pittet, B., Elmi, S., Mouterde, R., Cabral, M.-C., Comas-Rengifo, M., Gómez, J., Goy, A., Hesselbo, S.P., Jenkyns, H.H., Littler, K., Mailliot, S., Veiga de Oliveira, L.C., Osete, M. Luisa, Perilli, N., Pinto, S., Ruget, C., Suan, G., 2016. Base of the toarcian stage of the lower Jurassic defined by the global boundary stratotype section and point (GSSP) at the Peniche section (Portugal). *Episodes* 39, 460–481.
- Boulila, S., Galbrun, B., Huret, E., Hinnov, L.A., Rouget, I., Gardin, S., Bartolini, A., 2014. Astronomical calibration of the toarcian stage: implications for sequence stratigraphy and duration of the early Toarcian OAE. *Earth Planet. Sci. Lett.* 386, 98–111.
- Boussaha, M., Pittet, B., Mattioli, E., Duarte, L., 2014. Spatial characterization of the late Sinemurian (Early Jurassic) palaeoenvironments in the Lusitanian basin. *Palaeogeogr. Palaeoclimatol. Palaeoecol.* 409, 320–339.
- Bowman, C.N., Young, S.A., Kaljo, D., Eriksson, M.E., Them II, T.R., Hints, O., Martma, T., Owens, J.D., 2019. Linking the progressive expansion of reducing conditions to a stepwise mass extinction event in the late Silurian oceans. *Geology* 47, 968–972.
- Burgess, S.D., Bowring, S.A., Fleming, T.H., Elliot, D.H., 2015. High-precision geochronology links the Ferrar large igneous province with early-Jurassic ocean anoxia and biotic crisis. *Earth Planet. Sci. Lett.* 415, 90–99.
- De Lena, L.F., Taylor, D., Guex, J., Bartolini, A., Adatte, T., van Acken, D., Spangenberg, J.E., Samankassou, E., Vennemann, T., Schaltegger, U., 2019. The driving mechanisms of the carbon cycle perturbations in the late Pliensbachian (Early Jurassic). *Sci. Rep.* 9, 18430.
- Duarte, L.V., Oliveira, L., Comas-Rengifo, M.J., Silva, F., Silva, R.L., 2010. Organic-rich facies in the Sinemurian and Pliensbachian of the Lusitanian basin, Portugal: total organic carbon distribution and relation to transgressive-regressive facies cycles. *Geol. Acta* 8, 325–340.
- Fichtner, V., Strauss, H., Immenhauser, A., Buhl, D., Neuser, R.D., Niedermayr, A., 2017. Diagenesis of carbonate associated sulfate. *Chem. Geol.* 463, 61–75.
- Fike, D.A., Bradley, A.S., Rose, C.V., 2015. Rethinking the ancient sulfur cycle. *Annu. Rev. Earth Planet. Sci.* 43, 593–622.
- Filatova, N.I., Konstantinovskaya, E., Vishnevskaya, V., 2020. Jurassic-Lower Cretaceous siliceous rocks and black shales from allochthonous complexes of the Koryak-Western Kamchatka orogenic belt, East Asia. *Int. Geol. Rev.*, 1–20.
- Franceschi, M., Dal Corso, J., Cobiánchi, M., Roghi, G., Penasa, L., Picotti, V., Preto, N., 2019. Tethyan carbonate platform transformations during the Early Jurassic (Sinemurian–Pliensbachian, southern Alps): comparison with the late Triassic Carnian pluvial episode. *Geol. Soc. Am. Bull.* 131, 1255–1275.
- Franceschi, M., Dal Corso, J., Posenato, R., Roghi, G., Masetti, D., Jenkyns, H.C., 2014. Early Pliensbachian (Early Jurassic) C-isotope perturbation and the diffusion of the Lithiotis Fauna: insights from the western Tethys. *Palaeogeogr. Palaeoclimatol. Palaeoecol.* 410, 255–263.
- Garrels, R.M., Lerman, A., 1984. Coupling of the sedimentary sulfur and carbon cycles; an improved model. *Am. J. Sci.* 284, 989–1007.
- Garrels, R.M., Perry, E.A., 1974. Cycling of carbon, sulfur, and oxygen through geologic time. In: *The Sea*, vol. 5, pp. 303–336.
- Gill, B.C., Lyons, T.W., Frank, T.D., 2008. Behavior of carbonate-associated sulfate during meteoric diagenesis and implications for the sulfur isotope paleoproxy. *Geochim. Cosmochim. Acta* 72, 4699–4711.
- Gill, B.C., Lyons, T.W., Jenkyns, H.C., 2011a. A global perturbation to the sulfur cycle during the Toarcian Oceanic Anoxic Event. *Earth Planet. Sci. Lett.* 312, 484–496.
- Gill, B.C., Lyons, T.W., Young, S.A., Kump, L.R., Knoll, A.H., Saltzman, M.R., 2011b. Geochemical evidence for widespread euxinia in the Later Cambrian ocean. *Nature* 469, 80–83.
- Gomes, M.L., Hurtgen, M.T., Sageman, B.B., 2016. Biogeochemical sulfur cycling during Cretaceous oceanic anoxic events: a comparison of OAE1a and OAE2. *Paleoceanography* 31, 233–251.
- Guillot, S., Mahéo, G., de Sigoyer, J., Hattori, K.H., Pêcher, A., 2008. Tethyan and Indian subduction viewed from the Himalayan high- to ultrahigh-pressure metamorphic rocks. *Tectonophysics* 451, 225–241.
- Han, Z., Hu, X., BouDagher-Fadel, M., Jenkyns, H.C., Franceschi, M., 2021. Early Jurassic carbon-isotope perturbations in a shallow water succession from the Tethys Himalaya, southern hemisphere. *Newsl. Stratigr.* 54 (4), 461–481. <https://doi.org/10.1127/nos/2021/0650>.
- Han, Z., Hu, X., Kemp, D.B., Li, J., 2018. Carbonate-platform response to the Toarcian Oceanic Anoxic Event in the southern hemisphere: implications for climatic change and biotic platform demise. *Earth Planet. Sci. Lett.* 489, 59–71.
- Han, Z., Hu, X., Li, J., Garzanti, E., 2016. Jurassic carbonate microfacies and relative sea-level changes in the Tethys Himalaya (southern Tibet). *Palaeogeogr. Palaeoclimatol. Palaeoecol.* 456, 1–20.
- He, T., Dal Corso, J., Newton, R.J., Wignall, P.B., Mills, B.J.W., Todaro, S., Di Stefano, P., Turner, E.C., Jamieson, R.A., Randazzo, V., Rigo, M., Jones, R.E., Dunhill, A.M., 2020. An enormous sulfur isotope excursion indicates marine anoxia during the end-Triassic mass extinction. *Sci. Adv.* 6, eabb6704.
- He, T., Zhu, M., Mills, B.J.W., Wynn, P.M., Zhuravlev, A.Y., Tostevin, R., Pogge von Strandmann, P.A.E., Yang, A., Poulton, S.W., Shields, G.A., 2019. Possible links between extreme oxygen perturbations and the Cambrian radiation of animals. *Nat. Geosci.* 12, 468–474.
- Hesselbo, S.P., Jenkyns, H.C., 1998. British lower Jurassic sequence stratigraphy. British lower Jurassic sequence stratigraphy. In: *De Graciansky, P.-C., Hardenbol, J., Jacquint, T., Vail, P.R. (Eds.), Mesozoic and Cenozoic Sequence Stratigraphy of European Basins: SEPM Special Publication*, vol. 60, pp. 561–581.
- Hesselbo, S.P., Jenkyns, H.C., Duarte, L.V., Oliveira, L.C.V., 2007. Carbon-isotope record of the Early Jurassic (Toarcian) oceanic anoxic event from fossil wood and marine carbonate (Lusitanian basin, Portugal). *Earth Planet. Sci. Lett.* 253, 455–470.
- Holser, W.T., Clement, G.P., Jansa, L.F., Wade, J.A., 1988. Evaporite deposits of the North Atlantic rift. In: *Manspeizer, W. (Ed.), Developments in Geotectonics*. Elsevier, pp. 525–556. Chapter 22.
- Horita, J., Zimmermann, H., Holland, H.D., 2002. Chemical evolution of seawater during the Phanerozoic: implications from the record of marine evaporites. *Geochim. Cosmochim. Acta* 66, 3733–3756.
- Huang, C.J., Hesselbo, S.P., 2014. Pacing of the Toarcian Oceanic Anoxic Event (Early Jurassic) from astronomical correlation of marine sections. *Gondwana Res.* 25, 1348–1356.
- Huggett, J., Dennis, P., Gale, A., 2000. Geochemistry of early siderite cements from the Eocene succession of Whitecliff Bay, Hampshire Basin, UK. *J. Sediment. Res.* 70, 1107–1117.
- Jadoul, F., Berra, F., Garzanti, E., 1998. The Tethys Himalayan passive margin from Late Triassic to Early Cretaceous (South Tibet). *J. Asian Earth Sci.* 16, 173–194.
- Jenkyns, H.C., 2010. Geochemistry of oceanic anoxic events. *Geochim. Geophys. Geosyst.* 11, Q03004. <https://doi.org/10.1029/2009GC002788>.
- Jenkyns, H.C., 2020. The demise and drowning of Early Jurassic (Sinemurian) carbonate platforms: stratigraphic evidence from the Italian peninsula, Sicily and Spain. In: *L' Eredità Scientifica di Paolo Scandone, Geologo, Atti del Convegno Lincei*, vol. 335, pp. 55–82.
- Jenkyns, H.C., Jones, C.E., Grocke, D.R., Hesselbo, S.P., Parkinson, D.N., 2002. Chemostratigraphy of the Jurassic system: applications, limitations and implications for palaeoceanography. *J. Geol. Soc.* 159, 351–378.
- Jones, C.E., Jenkyns, H.C., Hesselbo, S.P., 1994. Strontium isotopes in Early Jurassic seawater. *Geochim. Cosmochim. Acta* 58, 1285–1301.
- Kampschulte, A., Strauss, H., 2004. The sulfur isotopic evolution of Phanerozoic seawater based on the analysis of structurally substituted sulfate in carbonates. *Chem. Geol.* 204, 255–286.
- Korte, C., Hesselbo, S.P., 2011. Shallow marine carbon and oxygen isotope and elemental records indicate icehouse-greenhouse cycles during the Early Jurassic. *Paleoceanography* 26, PA4219. <https://doi.org/10.1029/2011PA002160>.
- Korte, C., Hesselbo, S.P., Ullmann, C.V., Dietl, G., Ruhl, M., Schweigert, G., Thibault, N., 2015. Jurassic climate mode governed by ocean gateway. *Nat. Commun.* 6, 10015.
- Kump, L.R., Arthur, M.A., Patzkowsky, M.E., Gibbs, M.T., Pinkus, D.S., Sheehan, P.M., 1999. A weathering hypothesis for glaciation at high atmospheric pCO₂ during the Late Ordovician. *Palaeogeogr. Palaeoclimatol. Palaeoecol.* 152, 173–187.
- Luo, G., Kump, L.R., Wang, Y., Tong, J., Arthur, M.A., Yang, H., Huang, J., Yin, H., Xie, S., 2010. Isotopic evidence for an anomalously low oceanic sulfate concentration following end-Permian mass extinction. *Earth Planet. Sci. Lett.* 300, 101–111.
- Luo, G., Richoz, S., van de Schootbrugge, B., Algeo, T.J., Xie, S., Ono, S., Summons, R.E., 2018. Multiple sulfur-isotopic evidence for a shallowly stratified ocean following the Triassic-Jurassic boundary mass extinction. *Geochim. Cosmochim. Acta* 231, 73–87.
- Lyons, T.W., Gill, B.C., Shim, M.J., Frank, T.D., Hurtgen, M.T., Saltzman, M.R., Gellatly, A.M., Kah, L.C., 2004. Carbonate-associated sulfate as a paleoceanographic proxy: an update. *Geochim. Cosmochim. Acta* 68, A337.
- Marenco, P.J., Corsetti, F.A., Kaufman, A.J., Bottjer, D.J., 2008a. Environmental and diagenetic variations in carbonate associated sulfate: an investigation of CAS in the lower Triassic of the western USA. *Geochim. Cosmochim. Acta* 72, 1570–1582.
- Marenco, P.J., Corsetti, F.A., Hammond, D.E., Kaufman, A.J., Bottjer, D.J., 2008b. Oxidation of pyrite during extraction of carbonate associated sulfate. *Chem. Geol.* 247, 124–132.
- Markovic, S., Paytan, A., Wortmann, U.G., 2015. Pleistocene sediment offloading and the global sulfur cycle. *Biogeosci. Discuss.* 12, 3043–3060.
- Müller, T., Jurikova, H., Gutjahr, M., Tomašových, A., Schlögl, J., Liebetrau, V., Duarte, L.V., Milovský, R., Suan, G., Mattioli, E., Pittet, B., Eisenhauer, A., 2020. Ocean acidification during the early Toarcian extinction event: evidence from boron isotopes in brachiopods. *Geology* 12, 1184–1188.
- Newton, R.J., Reeves, E.P., Kafousia, N., Wignall, P.B., Bottrell, S.H., Sha, J.-G., 2011. Low marine sulfate concentrations and the isolation of the European epicontinental sea during the Early Jurassic. *Geology* 39, 7–10.
- Owens, J.D., Gill, B.C., Jenkyns, H.C., Bates, S.M., Severmann, S., Kuypers, M.M.M., Woodfine, R.G., Lyons, T.W., 2013. Sulfur isotopes track the global extent and dynamics of euxinia during Cretaceous Oceanic Anoxic Event 2. *Proc. Natl. Acad. Sci. USA* 110, 18407–18412.
- Percival, L.M., Ruhl, M., Hesselbo, S.P., Jenkyns, H.C., Mather, T.A., Whiteside, J.H., 2017. Mercury evidence for pulsed volcanism during the end-Triassic mass extinction. *Proc. Natl. Acad. Sci.* 114, 7929–7934.
- Percival, L.M.E., Witt, M.L.L., Mather, T.A., Hermoso, M., Jenkyns, H.C., Hesselbo, S.P., Al-Suwaidi, A.H., Storm, M.S., Xu, W., Ruhl, M., 2015. Globally enhanced Mercury deposition during the end-Pliensbachian extinction and Toarcian OAE: a link to the Karoo-Ferrar Large Igneous Province. *Earth Planet. Sci. Lett.* 428, 267–280.

- Present, T.M., Paris, G., Burke, A., Fischer, W.W., Adkins, J.F., 2015. Large carbonate associated sulfate isotopic variability between brachiopods, micrite, and other sedimentary components in Late Ordovician strata. *Earth Planet. Sci. Lett.* 432, 187–198.
- Price, G.D., Baker, S.J., VanDeVelde, J., Clemence, M.E., 2016. High-resolution carbon cycle and seawater temperature evolution during the Early Jurassic (Sinemurian–Early Pliensbachian). *Geochim. Geophys. Geosyst.* 17, 3917–3928.
- Raven, M.R., Fike, D.A., Bradley, A.S., Gomes, M.L., Owens, J.D., Webb, S.A., 2019. Paired organic matter and pyrite $\delta^{34}\text{S}$ records reveal mechanisms of carbon, sulfur, and iron cycle disruption during Ocean Anoxic Event 2. *Earth Planet. Sci. Lett.* 512, 27–38.
- Richardson, J.A., Keating, C., Lepland, A., Hints, O., Bradley, A.S., Fike, D.A., 2019. Silurian records of carbon and sulfur cycling from Estonia: the importance of depositional environment on isotopic trends. *Earth Planet. Sci. Lett.* 512, 71–82.
- Rosales, I., Quesada, S., Robles, S., 2006. Geochemical arguments for identifying second-order sea-level changes in hemipelagic carbonate ramp deposits. *Terra Nova* 18, 233–240.
- Ruhl, M., Hesselbo, S.P., Hinnov, L., Jenkyns, H.C., Xu, W., Riding, J.B., Storm, M., Minisini, D., Ullmann, C.V., Leng, M.J., 2016. Astronomical constraints on the duration of the Early Jurassic Pliensbachian stage and global climatic fluctuations. *Earth Planet. Sci. Lett.* 455, 149–165.
- Scotese, C., 2014. Atlas of Jurassic paleogeographic maps. In: PALEOMAP Atlas for ArcGIS, Volume 4, The Jurassic and Triassic, Maps 32–42. Mollweide Projection. PALEOMAP Project, Evanston, IL.
- Sellwood, B.W., 1971. The genesis of some sideritic beds in the Yorkshire Lias (England). *J. Sediment. Res.* 41, 854–858.
- Silva, R.L., Duarte, L.V., 2015. Organic matter production and preservation in the Lusitanian basin (Portugal) and Pliensbachian climatic hot snaps. *Glob. Planet. Change* 131, 24–34.
- Sim, M.S., Ono, S.H., Hurtgen, M.T., 2015. Sulfur isotope evidence for low and fluctuating sulfate levels in the Late Devonian ocean and the potential link with the mass extinction event. *Earth Planet. Sci. Lett.* 419, 52–62.
- Storm, M.S., Hesselbo, S.P., Jenkyns, H.C., Ruhl, M., Ullmann, C.V., Xu, W., Leng, M.J., Riding, J.B., Gorbanenko, O., 2020. Orbital pacing and secular evolution of the Early Jurassic carbon cycle. *Proc. Natl. Acad. Sci. USA* 117, 3974–3982.
- Suan, G., Mattioli, E., Pittet, B., Lecuyer, C., Sucheras-Marx, B., Duarte, L.V., Philippe, M., Reggiani, L., Martineau, F., 2010. Secular environmental precursors to Early Toarcian (Jurassic) extreme climate changes. *Earth Planet. Sci. Lett.* 290, 448–458.
- Suan, G., Pittet, B., Bour, I., Mattioli, E., Duarte, L.V., Mailliot, S., 2008. Duration of the Early Toarcian carbon isotope excursion deduced from spectral analysis: consequence for its possible causes. *Earth Planet. Sci. Lett.* 267, 666–679.
- Thode, H.G., Monster, J., 1970. Sulfur isotope abundances and genetic relations of oil accumulations in middle East basin. *Am. Assoc. Pet. Geol. Bull.* 54, 627–637.
- Turchyn, A.V., Schrag, D.P., 2006. Cenozoic evolution of the sulfur cycle: insight from oxygen isotopes in marine sulfate. *Earth Planet. Sci. Lett.* 241, 763–779.
- Turner, P., Pelz, K., 2017. Chapter 27 - development of an Upper Triassic-lower Jurassic evaporite basin on the Saharan platform, North Africa. In: Soto, J.L., Flinch, J.F., Tari, G. (Eds.), *Permo-Triassic Salt Provinces of Europe, North Africa and the Atlantic Margins*. Elsevier, pp. 581–599.
- Utrilla, R., Pierre, C., Orti, F., Pueyo, J.J., 1992. Oxygen and sulphur isotope compositions as indicators of the origin of Mesozoic and Cenozoic evaporites from Spain. *Chem. Geol.* 102, 229–244.
- Veizer, J., Holser, W.T., Wilgus, C.K., 1980. Correlation of $^{13}\text{C}/^{12}\text{C}$ and $^{34}\text{S}/^{32}\text{S}$ secular variations. *Geochim. Cosmochim. Acta* 44, 579–587.
- Wignall, P.B., Hallam, A., Newton, R.J., Sha, J.G., Reeves, E., Mattioli, E., Crowley, S., 2006. An eastern Tethyan (Tibetan) record of the Early Jurassic (Toarcian) mass extinction event. *Geobiology* 4, 179–190.
- Williford, K.H., Foriel, J., Ward, P.D., Steig, E.J., 2009. Major perturbation in sulfur cycling at the Triassic-Jurassic boundary. *Geology* 37, 835–838.
- Wotte, T., Shields-Zhou, G.A., Strauss, H., 2012. Carbonate-associated sulfate: experimental comparisons of common extraction methods and recommendations toward a standard analytical protocol. *Chem. Geol.* 326, 132–144.
- Xu, W., Ruhl, M., Jenkyns, H.C., Leng, M.J., Huggett, J.M., Minisini, D., Ullmann, C.V., Riding, J.B., Weijers, J.W., Storm, M.S., 2018. Evolution of the Toarcian (Early Jurassic) carbon-cycle and global climatic controls on local sedimentary processes (Cardigan Bay Basin, UK). *Earth Planet. Sci. Lett.* 484, 396–411.
- Yao, W., Wortmann, U.G., Paytan, A., 2019. Sulfur isotope – use for stratigraphy during times of rapid perturbations. In: Montenari, M. (Ed.), *Stratigraphy and Timescales*, vol. 4. Elsevier Academic Press, Amsterdam, pp. 1–33.